

This is the accepted manuscript made available via CHORUS. The article has been published as:

Multiparticle configurations of excited states in ^{155}Lu

R. J. Carroll *et al.*

Phys. Rev. C **94**, 064311 — Published 12 December 2016

DOI: [10.1103/PhysRevC.94.064311](https://doi.org/10.1103/PhysRevC.94.064311)

Multiparticle configurations of excited states in ^{155}Lu

R. J. Carroll,^{1,*} B. Hadinia,^{2,†} C. Qi,² D. T. Joss,¹ R. D. Page,¹ J. Uusitalo,³ K. Andgren,²
 B. Cederwall,² I. G. Darby,^{4,‡} S. Eeckhaudt,³ T. Grahn,³ C. Gray-Jones,³ P.T. Greenlees,³
 P. M. Jones,^{3,§} R. Julin,³ S. Juutinen,³ M. Leino,³ A. -P. Leppänen,^{3,¶} M. Nyman,^{3,**}
 J. Pakarinen,³ P. Rähkila,³ M. Sandzelius,^{3,2} J. Sarén,³ C. Scholey,³ D. Seweryniak,⁵ and J. Simpson⁶

¹*Oliver Lodge Laboratory, University of Liverpool, Liverpool, L69 7ZE, United Kingdom*

²*Royal Institute of Technology, Department of Physics, Alba Nova Centre, S-106 91 Stockholm, Sweden*

³*University of Jyväskylä, Department of Physics, FI-40014 Jyväskylä, Finland*

⁴*Oliver Lodge Laboratory, University of Liverpool, Liverpool L69 7ZE, United Kingdom*

⁵*Argonne National Laboratory, Argonne, Illinois 60439, USA*

⁶*STFC Daresbury Laboratory, Daresbury, Warrington WA4 4AD, United Kingdom*

(Dated: October 26, 2016)

Excited states in the neutron-deficient $N = 84$ nuclide ^{155}Lu have been populated using the $^{102}\text{Pd}(^{58}\text{Ni},\alpha\text{p})$ reaction. The ^{155}Lu nuclei were separated using the gas-filled recoil separator RITU and implanted into the Si detectors of the GREAT spectrometer. Prompt γ -ray emissions measured at the target position using the JUROGAM Ge detector array were assigned to ^{155}Lu through correlations with α decays measured in GREAT. Structures feeding the $(11/2^-)$ and $(25/2^-)$ α -decaying states have been revised and extended. Shell-model calculations have been performed and are found to reproduce the excitation energies of several of the low-lying states observed to within an average of 71 keV. In particular, the seniority inversion of the $25/2^-$ and $27/2^-$ states is reproduced.

PACS numbers: 23.20.Lv, 29.30.Kv, 21.10.Pc, 21.60.Cs

I. INTRODUCTION

The region above the $N = 82$ shell closure approaching the proton drip line features relatively small proton and neutron valence spaces due to the semi-magicity of ^{146}Gd , which can be considered to be an inert core for nuclei in this region. As such, this region is appropriate for the study of single-particle behaviour and the interactions between individual nucleons. This is particularly interesting as the orbitals available to the valence neutrons include the $h_{9/2}$ orbital, the spin-orbit partner to the $h_{11/2}$ orbital occupied by the valence protons.

Previous studies of isotones in this region have revealed that as the occupancy of the $\pi h_{11/2}$ orbital increases with increasing Z , states involving configurations with neutrons in the $h_{9/2}$ orbital are lowered in energy relative to those with neutrons in the $f_{7/2}$ orbital [1–4]. This observation has been attributed to an increasing attraction between $h_{11/2}$ protons and $h_{9/2}$ neutrons as the occu-

pancy of the $h_{11/2}$ proton orbital increases.

A particularly interesting feature observed in $N = 84$ isotones is the difference in the behaviour of the $27/2^-$ and $25/2^-$ states, both of which are thought to be a $\pi h_{11/2}^n \otimes \nu h_{9/2} f_{7/2}$ configuration [1]. The relatively constant behaviour of the $27/2^-$ state contrasts with the lowering in excitation energy with increasing Z observed in other states that feature an $h_{9/2}$ neutron [1]. The similarities between the behaviour of the $27/2^-$ state and those built on the $\pi h_{11/2} \otimes \nu f_{7/2}^2$ configuration have led to the proposal that a $(\pi h_{11/2}, \nu h_{9/2})_{1+}$ interaction, which is Pauli blocked in the $27/2^-$ state, is the dominant component lowering the states featuring an $h_{9/2}$ neutron [2].

The chain of $N = 84$ isotones crosses the proton drip line at ^{155}Lu [5]. Currently three α -decaying states are known in ^{155}Lu . Isomers having spin and parity $(1/2^+)$ and $(25/2^-)$ lie 20 keV and 1781 keV above the $(11/2^-)$ ground state, respectively [6–10]. The α -particle energies and half-lives of the states are, in order of increasing excitation energy, 5661(5) keV and 70(1) ms; 5586(5) keV and 136(9) ms; and 7390(5) keV and 2.71(3) ms [9, 10]. Yrast structures feeding the $(11/2^-)$ and $(25/2^-)$ states have been observed in previous work [1]. In this work the previous level scheme is revised and extended and nucleon configurations associated with these states are discussed. Experimental levels are compared with shell model calculations to aid the interpretation of assigned configurations.

*Present address: Department of Physics, University of Surrey, Guildford GU2 7XH, United Kingdom

†Present address: Department of Physics, University of Guelph, Guelph, Ontario, N1G 2W1 Canada

‡Present address: Department of Nuclear Sciences and Applications, International Atomic Energy Agency, A-1400 Vienna, Austria

§Present address: Department of Nuclear Physics, iThemba Laboratory for Accelerator Based Sciences, PO Box 722, Somerset West 7129, South Africa

¶Present address: STUK, Radiation and Nuclear Safety Authority, Finland

**Present address: Institute for Reference Materials and Measurements (IRMM), Retieseweg 111, B-2440 Geel, Belgium.

II. EXPERIMENTAL DETAILS

The experiment was performed at the Accelerator Laboratory at the University of Jyväskylä. Excited states in ^{155}Lu were populated in fusion-evaporation reactions in which a beam of accelerated ^{58}Ni ions, $E_{\text{beam}} = 255$ MeV, was incident on an isotopically enriched ^{102}Pd target foil of thickness ~ 1 mg cm^{-2} . An average beam intensity of 4.3 particle nA was delivered for 139 hours. Prompt γ rays were measured using the JUROGAM array, which comprised 43 Compton-suppressed Ge detectors focused on the target position. Scattered beam was suppressed by the RITU gas-filled separator [11, 12], which also transported recoiling reaction products to its focal plane where the GREAT spectrometer [13] was situated. Recoils that reached the focal plane passed through a multiwire proportional counter (MWPC) and implanted into the adjacently mounted double-sided silicon strip detectors (DSSDs). The recoil rate was approximately 2 kHz. Subsequent α decays were measured in the DSSDs. All detector signals were recorded by a triggerless data acquisition system [14], which time stamped them with a precision of 10 ns. The data were analysed using GRAIN [15] to produce ^{155}Lu γ -ray energy spectra using the Recoil Decay Tagging (RDT) technique [16, 17]. Where the statistics were sufficient, the data were sorted to produce $E_{\gamma 1} - E_{\gamma 2}$ γ -ray coincidence matrices, which were analysed using the RADWARE software package [18].

III. ANALYSIS

The energy spectrum of α decays measured in the DSSDs is shown in figure 1a. As can be seen in figure 1b, the region of the energy spectrum around 5661 keV, where the α -decay peak from the ground state is expected, contains significant levels of background from the low-energy tail of the ^{157}Hf α -decay peak. This results in the contamination from ^{157}Hf in the correlated γ -ray spectrum shown in figure 2a.

There is additional background in this spectrum arising from miscorrelations of ^{155}Lu α decays with ions that were implanted into the same DSSD pixel *after* the parent ^{155}Lu ion, but *before* the α decay. The 537 keV γ -ray transition from ^{157}Lu , which was abundantly produced in this experiment, is an example of this that appears in the spectrum (figure 2a). The relative contributions to the miscorrelation spectrum will depend not only on the available recoils and their production cross sections, but also on their α -decay half-lives. Those with shorter half-lives are more likely to α decay before the ^{155}Lu parent does, preventing the miscorrelation, thus they do not contribute as much to the background.

The background spectrum due to contamination was obtained by tagging on the characteristic ^{157}Hf α -decay energy, but with a recoil- α correlation time of 350 ms, as used to obtain the ^{155}Lu tagged spectrum. Correlating the recoil with γ rays in JUROGAM obtains a spec-

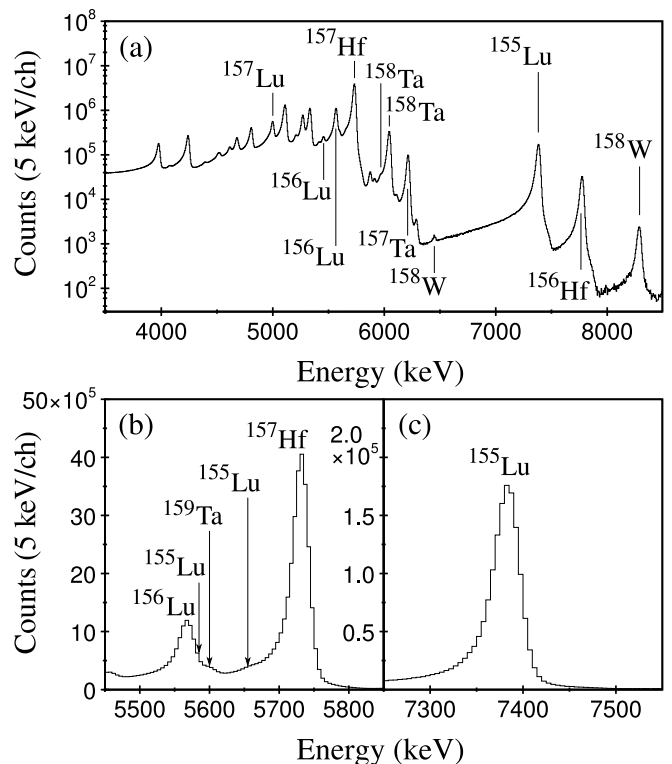


FIG. 1: (a) Energy spectrum of decays occurring within 700 ms of a recoil implantation in the same DSSD pixel. (b) The spectrum in (a) expanded around the α -decay peaks of the $(11/2^-)$ and $(1/2^+)$ states in ^{155}Lu . (c) The spectrum in (a) expanded around the α -decay peak of the $(25/2^-)$ state.

trum of background due to contamination. The background spectrum due to miscorrelation was obtained by tagging on recoil events that are followed by another recoil within the 350 ms correlation time. Correlating the *first* recoil with γ rays in JUROGAM produces a spectrum of background due to miscorrelation. These conditions effectively simulate the miscorrelation described above, producing a γ -ray background spectrum associated with recoils whose α -decay lifetimes are not so short as to prevent the miscorrelation occurring. The requirement that there are two recoils, rather than any single recoil that does not α decay for 350 ms, accounts for the variation in time difference between the implantation of the miscorrelated recoil and the ^{155}Lu α decay, which is dependent on the recoil rate.

The ratios of γ -ray transition intensities associated with background in the tagged spectra were used to determine the relative contributions of the two background spectra (contaminated and miscorrelated). The sum of the relative contributions formed a total background spectrum, which was then normalised to the tagged spectrum (figure 2a) and subtracted.

The resulting spectrum after correcting for these separate background contributions is shown in figure 2b, in which three γ -ray transitions can be seen with energies of 328.7(2) keV, 684.8(3) keV and 806.7(3) keV.

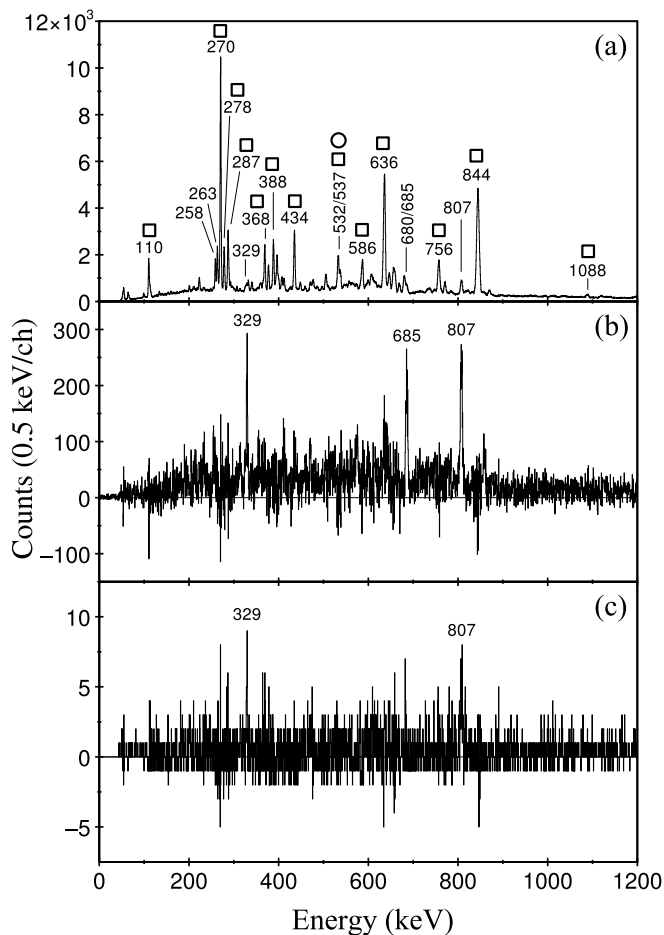


FIG. 2: (a) Energy spectrum of γ rays measured at the target position and correlated with recoils that were followed within 350 ms in the same DSSD pixel by an α decay with the energy expected for the $(11/2^-)$ ground state of ^{155}Lu . Peaks arising from contamination from ^{157}Hf and ^{157}Lu are indicated by the squares and circles, respectively. (b) As (a), after performing a background subtraction (see text for details). (c) Transitions in (b) in coincidence with the 685 keV γ ray.

The three γ -ray transitions are mutually coincident (coincidences with the 685 keV transition are shown in figure 2c) and form a single cascade feeding the $(11/2^-)$ ground state of ^{155}Lu , as shown in figure 3. The ordering of the transitions is based on their measured relative intensities, after correcting for the γ -ray detection efficiency, of $I(806.7) \equiv 1000$, $I(684.8) = 820(80)$ and $I(328.7) = 320(20)$. The 329 keV transition is observed for the first time in this work.

The 5586 keV α -decay peak of the $(1/2^+)$ isomeric state is also strongly contaminated by other α decays of similar energies (see figure 1b). This background and the low yield of these ^{155}Lu α decays rendered it impossible to obtain a sufficiently clean energy spectrum to allow γ rays populating this isomer to be identified.

The characteristic α -decay peak of the $(25/2^-)$ isomer at 7390 keV is relatively free of contamination (see fig-

ure 1c) and it is less susceptible to miscorrelations than the lower-lying states owing to its shorter half-life. A maximum correlation time of 14 ms between implanted ions and these α decays was applied and the energy spectrum of γ rays measured in JUROGAM in delayed coincidence with these ions is shown in figure 4a. The energies and intensities of these γ rays are presented in table I and the level scheme deduced on the basis of coincidence relationships and intensities is shown in figure 3.

The two strongest γ -ray transitions are those at 518 keV and 660 keV, and these were found to be in coincidence with all of the strong transitions in figure 4a. The placement of these transitions as the two lowest-lying transitions above the $(25/2^-)$ state is consistent with the previous work [1]. The third most intense γ ray has an energy of 212 keV and this was previously assumed to be the next transition in the sequence above the isomer and be of M1 multipolarity [1]. However, the 212 keV γ -ray transition is absent from the energy spectrum of γ rays observed in coincidence with the 1076 keV transition (see figure 4b), but both of these γ rays are in coincidence with the 798 keV transition (see figure 4c). In the level scheme presented in figure 3, the 212 keV and 1076 keV transitions are shown as populating the same state, which has the 798 keV γ ray as one of its de-exciting transitions. This interpretation is consistent with the γ rays that are observed in coincidence with the 560 keV transition (see figure 4d). Figures 4b and 4d provide evidence for the decay paths in parallel with the 798 keV transition that are presented in figure 3. These decay paths proceed via a 106 keV transition to the state depopulated by the 660 keV transition. The energy spectrum of γ rays observed in coincidence with the 106 keV transition is shown in figure 4e, which shows that this transition is in coincidence with γ rays placed higher in the level scheme such as the 560 keV, 382 keV, 545 keV and 550 keV transitions.

The observation of the 106 keV γ rays in JUROGAM means that it must be a dipole transition, because the lifetimes expected for higher multiplicities are too long. If it is of E1 multipolarity, the 106 keV transition intensity would be lower than those of higher-lying transitions after allowing for internal conversion [19]. However, an M1 multipolarity assignment would be compatible with the intensities of the other transitions in the level scheme and is therefore assumed for this transition.

The ordering of the 1076, 545 and 550 keV transitions was based on their relative intensities. While the 545 keV appears more intense than the 550 keV when observing coincidences with the 1076 keV transition (see figure 4b), the opposite is true in the singles spectrum (see figure 4a). This may be due to the presence of a second 550 keV transition elsewhere in the level scheme. An investigation of this transition has not yielded a convincing placement in the level scheme. The relative intensities of the 382 and 1212 keV transitions are consistent with each other. Their ordering has been chosen based on the likelihood that the breaking of a proton pair is required for this

TABLE I: Energies and efficiency corrected relative intensities of transitions observed at the target position in the structures feeding the $(25/2^-)$ state. Assigned multipolarities and internal conversion corrected [19] intensities are included. The transition marked with an asterisk (*) is an unresolved doublet, displaying a low level of coincidence with itself.

E_γ (keV)	I_γ	M λ	I_γ (ICC corrected)	E_γ (keV)	I_γ	M λ	I_γ (ICC corrected)	E_γ (keV)	I_γ	M λ	I_γ (ICC corrected)
106.3(1)	165(3)	(M1)	649(11)	443.3(2)	100(2)			797.5(3)	403(4)	(E2)	389(4)
212.1(2)	498(3)	(E1)	502(3)	513.0(2)	50(2)			958.5(3)	66(3)		
246.0(2)	45(1)			*518.5(2)	$\equiv 1000$	(M1)	$\equiv 1000$	997.5(4)	28(2)		
268.4(2)	22(1)			544.7(2)	119(2)			1054.2(4)	50(3)		
299.8(2)	108(2)			550.2(2)	231(3)			1076.2(4)	148(4)		
322.8(2)	38(2)			559.5(2)	353(4)			1122.4(5)	24(3)		
341.1(2)	172(2)			659.7(2)	1004(5)	(E1)	969(5)	1144.1(4)	33(2)		
354.2(2)	355(3)			681.9(5)	20(2)			1186.1(6)	21(3)		
381.5(2)	64(2)			687.0(3)	84(2)			1212.0(4)	64(3)		
397.9(2)	245(3)			696.0(3)	36(2)			1233.5(4)	91(3)		
416.2(2)	37(2)			709.2(3)	116(3)			1314.5(4)	110(3)		

configuration, a proton and a neutron in the $h_{11/2}$ and $h_{9/2}$ spin-orbit partner orbitals, respectively, would be expected to interact strongly due to their spatial overlap. The increase in proton number would increase the proton occupancy of the $h_{11/2}$ state, increasing the probability of an interaction between an $h_{11/2}$ proton and an $h_{9/2}$ neutron. The inclusion of a strong $[\pi h_{11/2}, \nu h_{9/2}]_{1+}$ interaction [2, 3] provides a mechanism for the observed lowering of the $25/2^-$ state relative to the $27/2^-$ state with increasing Z . This interaction is forbidden in the $27/2^-$ state, as it is not possible for a spin of $27/2$ to be constructed from the available angular momentum projections of the unpaired nucleons.

The $(29/2^+)$ and $(31/2^+)$ states are assumed to be a $\pi h_{11/2} \otimes \nu f_{7/2} i_{13/2}$ configuration, as adopted for the $N = 84$ isotones ^{151}Ho and ^{153}Tm [2, 3]. Higher-lying states could arise from the alignment of a pair of protons. Such assignments have been made in ^{153}Tm [3], where the $35/2^+$ state is assigned as a $\pi(h_{11/2})^4 d_{3/2} \otimes \nu(f_{7/2})^2$ configuration and the $37/2^-$ state is assigned as a $\pi(h_{11/2})^5 \otimes \nu f_{7/2} h_{9/2}$ configuration.

Shell model calculations have been performed for ^{155}Lu in the present work. An inert ^{146}Gd core was assumed and the model space took into account the proton $d_{3/2}$, $s_{1/2}$ and $h_{11/2}$ orbitals and the neutron $h_{9/2}$, $f_{7/2}$, $f_{5/2}$, $p_{3/2}$, $p_{1/2}$ and $i_{13/2}$ orbitals. The starting point for the calculation was the realistic charge-dependent Bonn nucleon-nucleon potential [23]. It was renormalized using the perturbative G-matrix approach in order to take into account the core polarisation effect [24]. The monopole part of the effective interaction thus obtained was further optimised by fitting to the excitation energies of 190 low-lying yrast states in $N = 82 - 86$ nuclides, in close proximity to ^{146}Gd , with a Monte Carlo optimisation procedure [25]. Parts of the multipole interaction matrix elements were adjusted following the description by A. Algora [26]. The single-particle energies of the proton orbitals were taken from experimental data: $\pi s_{1/2} = 0.0$ MeV, $\pi d_{3/2} = 0.253$ MeV, $\pi h_{11/2} = 0.0506$ MeV [27].

The single-particle energies used for the neutron orbitals were $\nu f_{7/2} = 0.0$ MeV, $\nu i_{13/2} = 0.997$ MeV, $\nu h_{9/2} = 1.397$ MeV. The unknown single-particle energies of the other neutron orbitals were determined by the fitting process. The calculations show that the experimental data can be reproduced by the optimised interaction within an average deviation of around 190 keV. The levels reproduced up to $31/2^+$ in ^{155}Lu have an average difference from the experimental levels of 71 keV, with a standard error of 22 keV and a largest deviation of 182 keV. The assumption that the ^{146}Gd core is inert is robust as core excitations would not be expected until much higher excitation energies than calculated here.

The experimental levels are reflected well in these calculations (see figure 6). Furthermore, the dominant components of the wavefunctions of the calculated states are consistent with the configurations deduced from the systematic trends. Further calculations have been performed, in which the anti-aligned $[\pi h_{11/2}, \nu h_{9/2}]_{1+}$ interaction matrix element has been switched off (see figure 6). The result is a significant increase in the excitation energy of the $25/2^-$ state, which has two notable effects: the $25/2^-$ state has a greater excitation energy than the $23/2^-$ state and thus would not be isomeric; and the difference in excitation energy between the $25/2^-$ and $27/2^-$ states is significantly reduced. In contrast, the excitation energy of the $27/2^-$ state changes very little with the removal of this interaction. This highlights the importance of the $[\pi h_{11/2}, \nu h_{9/2}]_{1+}$ interaction on the behaviour of the $25/2^-$ proton seniority $n = 3$ state.

Calculations in which the aligned $[\pi h_{11/2}, \nu h_{9/2}]_{10+}$ interaction is removed have also been performed (see figure 6). While the $\pi h_{11/2} \otimes \nu f_{7/2}$ states do not experience a significant change, those with a neutron in the $h_{9/2}$ orbital do. This reinforces the assignments of the $\pi h_{11/2} \otimes \nu f_{7/2}$ and $\pi h_{11/2} \otimes \nu f_{7/2} h_{9/2}$ configurations in this nucleus.

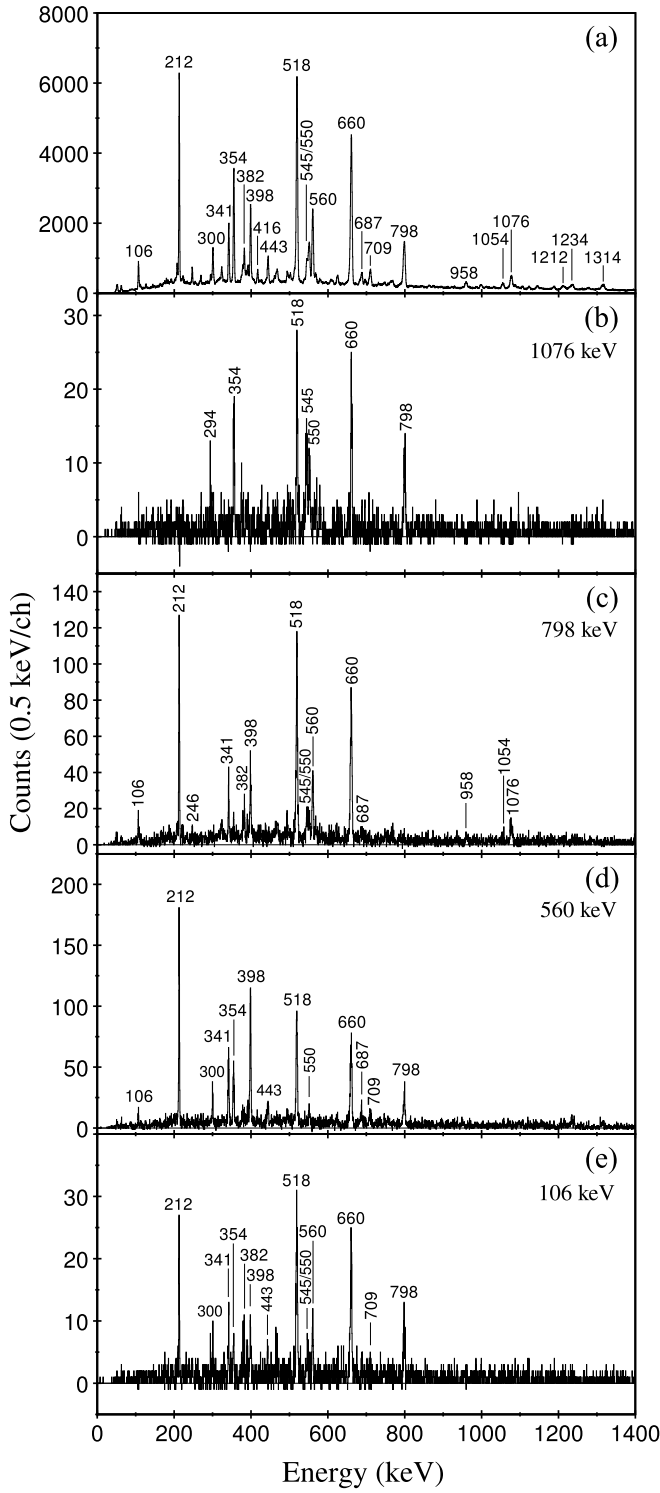


FIG. 4: (a) Energy spectrum of γ rays measured at the target position and correlated with recoils that were followed within 14 ms by an α decay of the $(25/2^-)$ state in ^{155}Lu in the same DSSD pixel. Energy spectra of these γ rays that were observed in coincidence with γ rays of energy (b) 1076 keV, (c) 798 keV, (d) 560 keV, and (e) 106 keV.

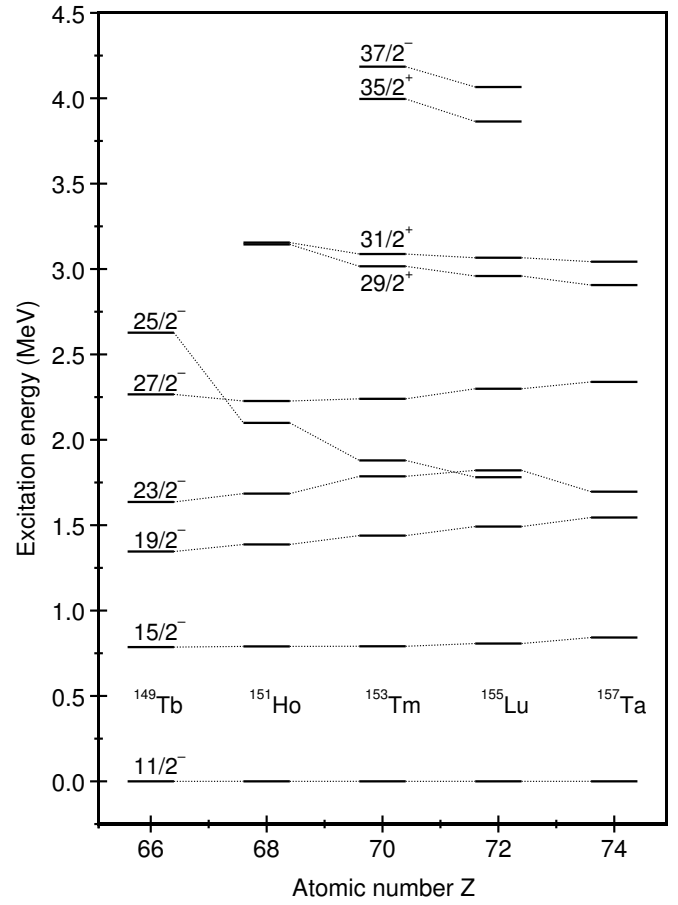


FIG. 5: Systematics of excited states in odd-A $N = 84$ isotones neighbouring ^{155}Lu , relative to the $(11/2^-)$ state. States up to $(23/2^-)$ follow a nearly constant trend across the isotones, whereas the $(25/2^-)$ state decreases in excitation energy with increasing Z [3, 20–22].

V. SUMMARY

Excited states in ^{155}Lu have been identified in an in-beam γ -ray spectroscopy experiment. An extended and revised level scheme has been proposed and compared with those of its odd-A $N = 84$ isotones. Shell model calculations optimised using empirical data from this region of the nuclear chart have been found to reproduce the experimentally observed states well. The importance of the anti-aligned 1^+ interaction between $h_{11/2}$ protons and $h_{9/2}$ neutrons on the behaviour of $25/2^-$ states has been demonstrated by these calculations.

Acknowledgments

This work has been supported through the UK Science and Technology Facilities Council (STFC), the Academy of Finland under the Finnish Centre of Excellence Programme 2006–2011 (Nuclear and Accelerator Based Physics contract 213503), EURONS (European Commis-

(a)	(b)			(c)			(d)		
				29/2 ⁻ 3586	31/2 ⁺ 3411		29/2 ⁻ 3943	31/2 ⁺ 3473	
(31/2 ⁺) 3066	29/2 ⁻ 3175	29/2 ⁺ 3141		29/2 ⁺ 3288			27/2 ⁻ 3057	29/2 ⁺ 3238	
(29/2 ⁺) 2959		31/2 ⁺ 3013					25/2 ⁻ 2969		
(27/2 ⁻) 2299	27/2 ⁻ 2280			27/2 ⁻ 2295					
(23/2 ⁻) 1822	23/2 ⁻ 1899	25/2 ⁻ 1782		23/2 ⁻ 1977	25/2 ⁻ 2214		23/2 ⁻ 1970		
(25/2 ⁻) 1781	19/2 ⁻ 1546			19/2 ⁻ 1504			19/2 ⁻ 1470		
(19/2 ⁻) 1493									
(15/2 ⁻) 807	15/2 ⁻ 826	Calculation: Full Hamiltonian		15/2 ⁻ 781	Calculation: 1+ interaction removed		15/2 ⁻ 747	Calculation: 10+ interaction removed	
(11/2 ⁻) 0	11/2 ⁻ 0			11/2 ⁻ 0			11/2 ⁻ 0		
Experiment	$\pi h_{11/2} \otimes$ $\nu(f_{7/2})^2$	$\pi h_{11/2} \otimes$ $\nu f_{7/2} h_{9/2}$	$\pi h_{11/2} \otimes$ $\nu f_{7/2} i_{13/2}$	$\pi h_{11/2} \otimes$ $\nu(f_{7/2})^2$	$\pi h_{11/2} \otimes$ $\nu f_{7/2} h_{9/2}$	$\pi h_{11/2} \otimes$ $\nu f_{7/2} i_{13/2}$	$\pi h_{11/2} \otimes$ $\nu(f_{7/2})^2$	$\pi h_{11/2} \otimes$ $\nu f_{7/2} h_{9/2}$	$\pi h_{11/2} \otimes$ $\nu f_{7/2} i_{13/2}$

FIG. 6: Comparison between (a) experimental levels and (b) shell model calculations for excited states in ^{155}Lu . Levels are labelled with spin, parity and excitation energy (keV). (c) Energy levels calculated with the anti-aligned 1^+ interaction turned off. The result is that most of the levels do not change drastically, except for the $25/2^-$ state, which significantly increases in excitation energy. (d) Calculations in which the aligned 10^+ interaction has been removed highlight states with a strong contribution from neutrons in the $\nu h_{9/2}$ orbital, which differ significantly from the calculations in (b).

sion contract no. RII3-CT-2004-506065) and the U.S. Department of Energy, Office of Nuclear Physics, under contract No. DEAC02-06CH11357. The UK/France (STFC/IN2P3) Loan Pool and GAMMAPOOL network are acknowledged for the EUROGAM detectors of JUROGAM. T.G., P.T.G. and C.S. acknowledge the support of the Academy of Finland, contract numbers 131665, 111965 and 209430, respectively. The authors gratefully acknowledge the efforts of the accelerator and technical staff.

-
- [1] K. Y. Ding, J. A. Cizewski, D. Seweryniak, H. Amro, M. P. Carpenter, C. N. Davids, N. Fotiades, R. V. F. Janssens, T. Lauritsen, C. J. Lister, et al., *Phys. Rev. C* **64**, 034315 (2001).
- [2] C. T. Zhang, P. Kleinheinz, M. Piiparinen, R. Collatz, T. Lonnroth, G. Sletten, and J. Blomqvist, *Z.Phys.A* **348**, 65 (1994).
- [3] C. T. Zhang, P. Kleinheinz, M. Piiparinen, R. Collatz, T. Lonnroth, G. Sletten, and J. Blomqvist, *Z.Phys.A* **348**, 249 (1994).
- [4] C. T. Zhang, R. Broda, R. Menegazzo, P. Kleinheinz, R. Collatz, H. Grawe, S. Hofmann, M. Lach, K. H. Maier, M. Schramm, et al., *Z. Phys. A* **345**, 327 (1993).
- [5] G. Audi, A. H. Wapstra, and C. Thibault, *Nucl. Phys. A* **729**, 337 (2003).
- [6] R. D. Macfarlane, *Phys.Rev.* **137**, 1448 (1965).
- [7] S. Hofmann, W. Faust, G. Münzenberg, W. Reisdorf, and P. Armbruster, *Z. Phys. A* **291**, 53 (1979).
- [8] S. Hofmann, P. Armbruster, G. Berthes, T. Faestermann, A. Gillitzer, F. P. H. berger, W. Kurcewicz, G. Münzenberg, K. Poppensieker, H. J. Schött, et al., *Z. Phys. A* **333**, 107 (1989).
- [9] C. N. Davids, P. J. Woods, J. C. Batchelder, C. R. Bingham, D. J. Blumenthal, L. T. Brown, B. C. Busse, L. F. Conticchio, T. Davidson, S. J. Freeman, et al., *Phys. Rev. C* **55**, 2255 (1997).
- [10] R. D. Page, P. J. Woods, R. A. Cunningham, T. Davinson, N. J. Davis, A. N. James, K. Livingston, P. J. Sellin, and A. C. Shotton, *Phys. Rev. C* **53**, 660 (1996).
- [11] M. Leino, J. Äystö, T. Enqvist, P. Heikkinen, A. Jokinen, M. Nurmia, A. O. W. H. Trzaska, J. Uusitalo, K. Eskola, P. Armbruster, et al., *Nucl. Instr. and Meth. B* **99**, 653 (1995).
- [12] J. Uusitalo, P. Jones, P. Greenlees, P. Rahkila, M. Leino, A. N. Andreyev, P. A. Butler, T. Enqvist, K. Eskola, T. Grahn, et al., *Nucl. Instr. and Meth. B* **204**, 638 (2003).
- [13] R. D. Page, A. N. Andreyev, D. E. Appelbe, P. A. Butler, S. J. Freeman, P. T. Greenlees, R.-D. Herzberg, D. G. Jenkins, G. D. Jones, P. Jones, et al., *Nucl. Instr. and Meth. B* **204**, 634 (2003).
- [14] I. H. Lazarus, D. E. Appelbe, P. A. Butler, P. J. Coleman-Smith, J. R. Cresswell, J. S. Freeman, R. D. Herzberg, I. Hibbert, D. T. Joss, S. C. Letts, et al., *IEEE Trans. Nucl. Sci.* **48**, 567 (2001).
- [15] P. Rahkila, *Nucl. Instr. and Meth. A* **595**, 637 (2008).
- [16] K.-H. Schmidt, R. S. Simon, J.-G. Keller, F. P. Hessberger, G. Münzenberg, B. Quint, H.-G. Clerc, W. Schwab, U. Gollerthan, and C.-C. Sahm, *Phys. Lett.* **168B**, 39 (1986).
- [17] E. S. Paul, P. J. Woods, T. Davinson, R. D. Page, P. J. Sellin, C. W. Beausang, R. M. Clark, R. A. Cunningham, S. A. Forbes, D. B. Fossan, et al., *Phys.Rev.* **C51**, 78 (1995).
- [18] D. Radford, *Nucl. Instrum. Methods Phys. Res. A* **361**, 297 (1995).
- [19] T. Kibédi, T. W. Burrows, M. B. Trzhaskovskaya, P. M. Davidson, and C. W. N. Jr., *Nucl. Instr. and Meth. A* **589**, 202 (2008).
- [20] M. Lach, P. Kleinheinz, M. Piiparinen, M. Ogawa, S. Lunardi, M. C. Bosca, J. Styzcen, and J. Blomqvist, *Z. Phys. A* **341**, 25 (1991).
- [21] J. Gizon, A. Gizon, S. André, J. Genevey, J. Jastrzebski, R. Kossakowski, M. Moszynski, and Z. Preibisz, *Z. Phys. A* **301**, 67 (1981).
- [22] D. Seweryniak, J. Uusitalo, P. Bhattacharyya, M. P. Carpenter, J. A. Cizewski, K. Y. Ding, C. N. Davids, N. Fotiades, R. V. F. Janssens, T. Lauritsen, et al., *Phys. Rev. C* **71**, 054319 (2005).
- [23] R. Machleidt, *Phys. Rev. C* **63**, 024001 (2001).
- [24] M. Hjorth-Jensen, T. T. S. Kuo, and E. Osnes, *Phys. Rep.* **261**, 125 (1995).
- [25] C. Qi and Z. X. Xu, *Phys. Rev. C* **86**, 044323 (2012).
- [26] A. Algora, B. Rubio, D. Cano-Ott, J. L. Taín, A. Gadea, J. Agramunt, M. Gierlik, M. Karny, Z. Janas, A. Plochocki, et al., *Phys. Rev. C* **68**, 034301 (2003).
- [27] *National Nuclear Data Center*, information extracted from the NuDat 2 database, <http://www.nndc.bnl.gov/nudat2/>.